Toward Nanoscale Engineering of Triacylglycerol Crystal Networks

ARTICLE *in* CRYSTAL GROWTH & DESIGN · JULY 2010

Impact Factor: 4.89 · DOI: 10.1021/cg100469x

2 AUTHORS:

Nuria Acevedo
Iowa State University
24 PUBLICATIONS **308** CITATIONS
SEE PROFILE

Alejandro Gregorio Marangoni
University of Guelph
344 PUBLICATIONS **6,885** CITATIONS
SEE PROFILE

DOI: 10.1021/cg100469x

CRYSTAL GROWTH & DESIGN Article
2010, Vol. 10
3334–3339

Toward Nanoscale Engineering of Triacylglycerol Crystal Networks

Nuria C. Acevedo and Alejandro G. Marangoni*

Guelph-Waterloo Physics Institute, Centre for Food & Soft Materials Science, Department of Food Science, University of Guelph, 50 Stone Road East, Guelph, Ontario, Canada, N1G 2W1

Received April 8, 2010; Revised Manuscript Received June 11, 2010

ABSTRACT: Cryogenic transmission electron microscopy and X-ray diffraction techniques were used to analyze the effect of crystallization conditions on the nanostructure of triacylglycerol crystal networks. Nanoplatelet size was strongly affected by composition and degree of supersaturation in the melt, as well as external fields during crystallization, such as cooling and shear rate. Chemical interesterification induced a decrease in nanoplatelet size, while increases in the solid mass fraction also resulted in a decrease in nanoplatelet dimensions. Fast cooling rates and crystallization under shear produced a significant decrease in platelet length, width, and thickness. This work opens up the possibility of judiciously engineering the nanoscale of fat-structured products in order to formulate products with specific functionalities including hardness, liquid oil binding, water vapor barrier properties, and metabolic response in humans.

Introduction

Traditional high-fat food products such as ice cream, butter, and chocolate achieve their semisolid structure from hardstock lipids, which rely on trans and saturated fats to provide their desired functional properties. However, excessive consumption of trans and saturated fatty acids is strongly associated with deleterious health factors such as adverse effects on lipoprotein (cholesterol) profiles, increased incidence of heart disease, and metabolic syndrome.[1−4] Consequently, over the past several decades, increasing emphasis has been placed on eliminating unhealthy fats from our diets. It seems simple enough, but the process of eliminating saturated and trans fat may jeopardize the functional properties of the final product; therefore, it has become necessary to learn how to structure these fat-based food materials with less crystalline material. This has given researchers the challenge of developing a deeper understanding of fat crystal structure since it plays an important role in the final properties of fats. Several studies have revealed that the structure of plastic fats consists of a continuous fractal network of crystalline fat suspended in an oil phase.[5−11] The growth of this crystalline network starts when the triacylglycerol (TAG) molecules present in the sample arrange and crystallize from the melt, through a continuous aggregation process, into polycrystals (∼1−3 μm) and crystal aggregates (∼20−100 μm).

In our previous work, we employed the cryo-TEM technique in order to visualize the nanostructure of a fat crystal network. We introduced a new method, based on a previous work from Chawla and deMan,[11] where the oil phase is extracted through subsequent steps of washing with a cold solvent and mechanical disruption of the crystalline network. Additionally, we carried out small-angle X-ray diffraction experiments and applied Scherrer analysis to the obtained patterns to determine dimension of the primary crystals represented by the domain size.[12] As a result, we were able to visualize and characterize the "primary crystals" of a tristearin crystalline network as asymmetric nanoplatelets (∼150 nm × 60 nm × 30 nm), formed by the epitaxial stacking of TAG lamellae.

*Corresponding author. Telephone: +1-519-824-4120 x54340; fax: +1-519-824-6631; e-mail: amarango@uoguelph.ca.

It is well-known that several factors influence the process of lipid crystallization, in particular the way in which the sample is cooled from the melt (cooling rate, initial and final temperatures, agitation or shear rate) and the composition (fatty acids profile and TAG organization). The shape and size of the crystalline particles in the fat network depend strongly on the crystallization conditions.[13]

Chemical interesterification is a method used to modify the physicochemical characteristics of oils and fats.[14] The TAG groups present in fats and oils have specific requirements as to activation energy for molecular diffusion and formation of stable crystalline nuclei in the crystallization process.[15] During interesterification, fatty acids are exchanged within and among triacylglycerols, until a thermodynamic equilibrium is reached.[16] As a consequence of this modification, the related energetic requirement is altered, and changes occur in crystal growth velocity and size.[17] Interesterification thus produces significant modifications in the crystallization properties of oils and fats by increasing the number of TAG species present and altering intersolubility among the TAG molecules.[18,19]

The purpose of this work was to analyze the effects of composition (by interesterification) and external fields (by changes in cooling and shear rate during crystallization), on the nanostructure in binary fat blends of fully hydrogenated canola oil (FHCO) and high oleic sunflower oil (HOSO). The induced modifications at the nanoscale of the TAG crystal networks were evaluated by cryogenic transmission electron microscopy (cryo-TEM) and small-angle X-ray diffraction (SAXRD). Our findings will be the initial steps in the development of a qualitative and quantitative understanding of the relationship between the nanostructure (never considered before) and the macroscopic properties in fat crystal networks. The ultimate goal is to be able to engineer the nanostructure of edible fats so as to achieve desirable organoleptic properties in fat-structured food formulations.

Experimental Section

Materials. Fully hydrogenated canola oil (FHCO) and high oleic sunflower oil (HOSO) were generously provided by Bunge Canada (Toronto, Canada) and Nealanders (Toronto, Canada), respectively. All chemicals and organic solvents were purchased from

Published on Web 07/08/2010

Table 1. Melting Temperatures (T_m), Enthalpies of Melting (ΔH_m) and Solid Mass Fractions (SMF) for Non-Interesterified and Chemically Interesterified Blends of FHCO and HOSO

% FHCO[a]		20	30	40	50	60	70	80	90	100
NI blends	T_m (K)	333.3	336.5	337.4	338.8	340.7	342.0	344.2	344.4	344.9
	ΔH_m(kJ mol^{-1})[b]	32.5	61.4	73.4	95.4	106.8	120.3	129.6	148.4	164.9
	SMF[c]	0.15	0.21	0.29	0.39	0.50	0.61	0.74	0.86	0.98
CI blends	T_m (K)	316.4	319.4	326.3	328.5	330.7	335.4	336.6	339.1	340.9
	ΔH_m(kJ mol^{-1})[b]	4.9	12.6	15.9	30.7	40.9	74.8	83.7	124.6	154.7
	SMF[c]	0.004	0.03	0.07	0.13	0.28	0.43	0.67	0.85	0.98

[a] % of fully hydrogenated canola oil. [b] Considering tristearin (FHCO) MW = 891.48 g mol^{-1}, %SD < 2.5% [c] Solid mass fraction (SFC/100), %SD < 0.1%

Fisher Scientific and Sigma-Aldrich (ON, Canada). Ahmadi et al.[20] reported the fatty acid composition of FHCO and HOSO. FHCO contained ~88% stearic acid (18:0), ~9% of palmitic acid (16:0), and ~2% arachidic acid (20:0). The predominant fatty acids in HOSO were oleic acid (18:1), ~77%, while only small amounts of linoleic acid (18:2), stearic acid, and palmitic acid were present, ~8%, ~6%, and~5%, respectively.

Blend Preparation. Blends of FHCO and HOSO were mixed in 10% increments (w/w) ranging from 20% to 100% of hardstock. The blends were held at 80 °C for 30 min to erase crystal memory followed by storage at a temperature 40 °C higher than the corresponding melting temperature (T_m) of the particular blend (Table 1) in order to promote the β polymorphic (triclinic) form. X-ray diffraction patterns were collected at 20 °C to confirm the presence of the signals corresponding to the desired polymorphic form. Subsequently, blends were kept at 20 °C prior to analysis.

Chemical interesterification was carried out according to the method described by Ahmadi et al.[21] 0.3% (w/w) sodium methoxide (Sigma-Aldrich, Ontario, Canada) was used as a catalyst. Five hundred grams of each blend were melted in a glass container at 85 °C, under a nitrogen layer to limit moisture and air. The chemical reaction was started by the addition of 1.5 g of catalyst. The blends were interesterified under bubbling nitrogen for 60 min at 88 ± 2 °C. The start of the reaction was associated with the appearance of a red-brown color. The reaction was terminated by adding 4% acidic water (20% citric acid, w/v). The interesterified samples were carefully washed with 8 parts of hot water (1:8) to remove soaps, excess citric acid, sodium methoxide, and free fatty acids. Residual water was then removed by adding sodium sulfate (5%). Bleaching clay (1.5 wt %) was added and the sample was heated again at 88 ± 2 °C for 20 min under nitrogen gas. The interesterified blend was then vacuumed filtered through a hot Buchner funnel using Whatman filter paper no. 4. The fat was poured into a glass container and stored at 5 °C prior to use.

In order to analyze the effects of the external field conditions 1:1 (w/w) mixtures of FHCO and HOSO crystallized at two different cooling rates (1 and 10 °C/min) and isothermally at two different shear rates (statically and 300 s^{-1}). Shear experiments were carried out in a Couette shear cell as previously described.[22]

Differential Scanning Calorimetry (DSC). A differential scanning calorimeter (DSC; Q1000, TA Instruments, Mississauga, ON, Canada) was used in the thermal analysis of the different fat blends. The instrument heat capacity response was calibrated with sapphire, and the heat flow was calibrated with indium. Approximately 10 mg of the fat sample was placed in alodined pans and sealed hermetically (an empty pan served as reference). All measurements were performed at a heating rate of 5 °C/min. Thermograms were evaluated using TA Instruments Universal Analysis Software. The peak melting temperature (T_m) and the enthalpy of melting (ΔH_m) were determined. The average and standard deviation of four replicates are reported in this study.

Solid Fat Content (SFC). SFC before and after interesterification were measured by pulsed nuclear magnetic resonance (pNMR), (Bruker, Milton, ON, Canada). The blends were held at 80 °C for 30 min to erase crystal memory followed by storage at a temperature 40 °C higher than the corresponding melting temperature (T_m) of the particular blend (Table 1) in order to promote the β polymorphic (triclinic) form. Samples were kept at 20 °C until the moment of the SFC determination.

Powder X-ray Diffraction Analysis (XRD). XRD data were collected using a Rigaku Multiflex Powder X-ray diffractometer (Rigakug, Japan). The copper lamp (λ = 1.54 Å for copper) was set to 40 kV and 44 mA. A 0.57 divergence slit, 0.57 scatter slit, and 0.3 mm receiving slit were used. For the small-angle X-ray diffraction analysis (SAXD), the samples were scanned from 0.9 to 8 deg at 0.02°/min. The wide-angle X-ray diffraction analysis (WAXD) was carried out scanning the samples from 16 to 35 deg at 0.5°/min. PeakFit software (Seasolve, Framingham, MA, USA) was used to analyze the obtained patterns in both SAXD and WAXD.

From the SAXD patterns, the crystalline domain size (ξ) can be calculated by the well-known Scherrer formula which is limited to nanoscale particles and it is not applicable to sizes larger than about 100 nm:[12]

$$\xi = \frac{K\lambda}{\text{fwhm}\cos(\theta)}$$

where K is the shape factor, θ is the diffraction angle, fwhm is the full width at half of the maximum peak height in radians (usually from the first small angle reflection corresponding to the (001) plane), and λ is the wavelength of the X-ray. The dimensionless shape factor provides information about the "roundness" of the particle. For a spherical particle the shape factor is 1, and for all other particles it is smaller than 1. A value of 0.9 is usually used for crystallites of unknown shape and is the magnitude employed in this study.

Cryo-TEM. In order to discard oil fraction and favor single crystals observation, fat blends were treated at 10 °C as follows. Fat samples were suspended in cold isobutanol approximately in the ratio 1:50 using a glass stirring rod to obtain a uniform suspension. The fat + isobutanol mixtures were homogenized at 30 000 rpm with a rotostator (Power Gen 125, Fisher Scientific) for 10 min. Then, the crystals were collected by vacuum filtration through a glass fiber filter of 1.0 μm pore size. After filtration, the recovered solid was resuspended in cold isobutanol and rehomogenized for 10 min using the rotostator in order to obtain a suitable dispersion of crystals. Finally, the mixtures were sonicated at 10 °C for 60 min using an ultrasonic processor (Bransonic 1210R-DTH, Branson Ultrasonic Corporation, Danburry, CT, USA) to complete the dispersion of the fat crystals. Assuming Couette type flow at the rotostator tip (radius = 3 mm, gap size = 200 μm), we estimated a tip shear rate of 47 000 s^{-1}. The Peclet number is the ratio between the shear rate and the rotational diffusivity of an object in that shear field, D_r, where $D_r = 3k_BT/\pi\eta d_p^3$. Assuming that in order to align that object in the shear field, a 10-fold larger shear rate relative to the rotational diffusivity is required, for a spherical particle of diameter d_p = 100 nm, a shear rate of 112 000 s^{-1} would then be required (T = 283 K, isobutanol viscosity, η = 0.0033 Pa s, $k_B = 1.38 \times 10^{-23}$ J/K). Thus, the shear rate chosen is high enough to break low micrometer-scale objects, but not too high to disrupt nanometer-scale objects.

Five microliters of dispersion were placed on a copper grid with perforated carbon film (Canemco-Marivac, Quebec, Canada), and excess liquid was blotted automatically for 2 s using filter paper. A staining aqueous solution of 2% of uranyl acetate was used to enhance contrast. Subsequently, the sample was transferred to a cryo-holder (Gatan Inc., Pleasanton, CA, USA) for direct observation at −176 °C in a FEI Tecnai G2 F20 energy-filtered Cryo-TEM operated at 200 kV in low dose mode. The blurring effect on micrographs caused by inelastically scattered electrons is eliminated by energy filtering which improves image contrast. Zero-loss energy-filtered images were taken using a Gatan 4k CCD camera. Micrographs were stored and analyzed using DigitalMicrograph software

(USA). Image J 1.42q software (USA) was employed for a semiautomatic analysis procedure.

Statistical Analysis. Data were processed using GraphPad Prism 5 software (GraphPad Software, Inc., San Diego, CA, USA). Values reported correspond to the means and standard errors of the determinations. A student t test was used to evaluate statistical significance in the observed changes in crystal dimensions. All statistical tests were two-tailed with a P-value < 0.05 taken to indicate statistical significance.

Results and Discussion

Many studies have related the effect of the crystallization conditions on the structure of fats;[21,23−30] however, until today, no systematic studies on the effects of external fields on the nanostructure of fat crystal networks existed.

It is well know that the macroscopic functionality and physical properties of polycrystalline materials can be strongly affected by alterations in crystal size distribution and the arrangement of these crystals in space. Moreover, both factors, size and aggregation state of the crystals, depend on crystallization kinetics, which are in turn strongly influenced by the supersaturation in the melt. However, the supersaturation of a multicomponent system, like a chemically interesterified mixture of tristearin and triolein, is hard to define since there is not a single high melting component in the melt, but rather several crystallizing species with different melting points and molar enthalpies of fusion. To make matters worse, the relative proportion of the crystallizing species varies depending on the blend proportions. Therefore, a key parameter for describing the effective supersaturation of a chemically interesterified mixture is the final amount of solids, solid fat content (SFC) or solid mass fraction (solid fat content/100). Thus, instead of discussing changes in TAG crystal structure as a function of supersaturation ($\ln \beta$) as was defined by Acevedo and Marangoni,[31] here we discuss changes in network structure as a function of the final solid mass fraction. The solid mass fraction of the blends at 20 °C determined by low resolution pNMR are listed in Table 1. The melting temperatures (T_m) and molar enthalpies of melting (ΔH_m) determined by DSC are reported in Table 1 as well. Interesterification caused a significant decrease in the solid mass fraction ($P < 0.0001$) in all binary blends. Analogous results were observed by Ahmadi et al.[21] working with similar non-interesterified and chemically interesterified fat blends. They attributed the decrease in the solid mass fraction to a reduction of the amount of tristearin in interesterified samples. According to Campos,[32] crystallization enthalpy value is strongly related to the intermolecular arrangement of TAG species and, therefore, usually modified by randomization. In this case, the values of molar enthalpy of melting decreased in all the samples after randomization (Table 1) which also may be related to the lower proportion of tristearin in these blends.

Figure 1a,b shows the platelet lengths and widths, respectively, obtained from the image analysis of the cryo-TEM images for non-interesterified (NI) and chemically interesterified (CI) fat blends. The information acquired from crystallization of the samples under static or sheared conditions is displayed as well. Changes in solid fat content (or solid mass fraction), in this case an indicator of the supersaturation of the melt, influence how the crystalline network is structured. Therefore, since there is a solid mass fraction change intrinsic to the process of interesterification, equal solid mass fraction contents were plotted in Figure 1, even though if they correspond to different FHCO−HOSO proportions (Table 1).

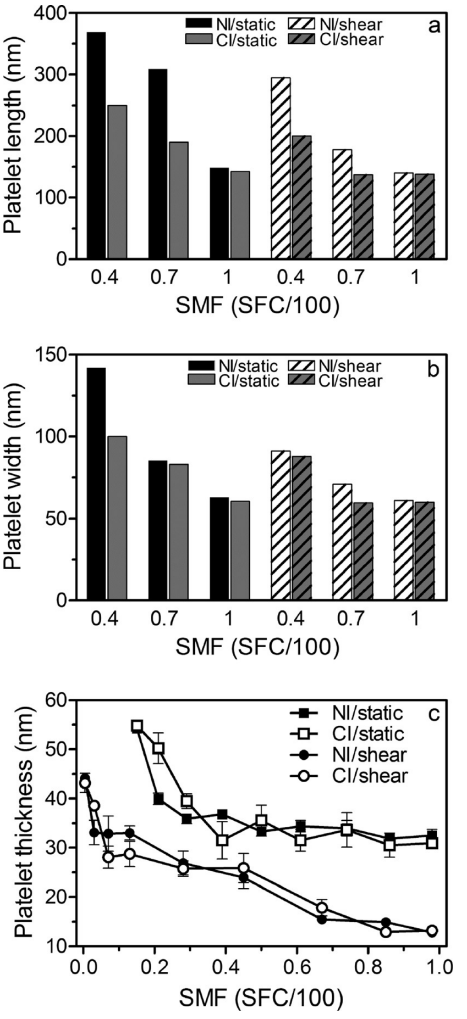

Figure 1. Effects of solid mass fraction (SMF), composition, and external fields on the nanostructural level. Platelet lengths (a) and widths (b) obtained by analysis of the cryo-TEM micrographs of FHCO/HOSO blends, with the three selected solid mass fraction values, before and after interesterification and crystallized statically or under shear. (c) Platelet thickness, obtained by the Scherrer analysis of the X-ray data, for blends crystallized statically or under shear as a function of solid mass fraction. In (a) and (b) the standard error is ≤1.5% in all samples. In (c) the error bars represent the standard deviation of the average thickness value.

Nanoplatelet dimensions in blends with solid mass fractions of approximately 0.4, 0.7, and 1 are represented in Figure 1; however, experiments were carried out along the whole range of hardstock proportion with results showing an analogous tendency to that reported here.

Interesterification caused significant reduction in nanoplatelet size in all the binary blends. This effect was probably due to the incorporation of stearic acid into triolein TAGs, thus creating intermediate TAG species such as OOS, OSO, SOS, and SSO. These new TAGs would now also have ability to nucleate, thus leading to the creation of a greater number of crystals. At similar supersaturations, this will lead to a smaller platelet size distribution in the interesterified blends. Numerous authors have previously analyzed the microstructural aspects of interesterified fats.[33−35] While those studies only focused on the micro (or meso) scale, the results also showed similar decreases in crystal size upon interesterification.

Our results show that there is a significant decrease in nanoplatelet dimensions with an increase in solid mass fraction

(Figure 1). Some authors observed similar behavior at the mesoscale when the proportion of oil in fat blends increased.[24,35] According to Himavan et al.[36] when solid fat content decreases (oil content increases), lower viscosity of the melt enhances molecular mobility resulting in larger crystals. This supersaturation effect, manifested as a reduction in nanoplatelet size, can be observed in all the samples independent of their composition and crystallization conditions. As an example, the results show that in statically crystallized blends, a change in solid mass fraction from 0.4 to 1.0 leads to a decrease in platelet lengths and widths of approximately 60% and 40% for NI and CI blends, respectively (Figure 1a,b).

The effects of shearing during the crystallization process have been studied extensively.[22,37−41] In this work, in order to analyze the effect of crystallization under shear on the nanostructure of TAG crystal networks, crystallization experiments in presence and absence of laminar shear were carried out for all the blends. Figure 1a,b shows the effect of crystallization under different shear rates, which resulted in a decrease in platelet length and width. It has been recognized that shear can enhance the kinetics of nucleation since it increases mass transfer in the melt.[22,42,43] As a consequence, it is predictable to observe smaller sized crystals, since a high nucleation density and a low crystal growth rate predominated during the crystallization process. As expected, laminar shear induced the formation of smaller nanoplatelets ($P < 0.001$) as can be observed in Figure 1a,b. Nanoplatelet lengths and widths decreased from 4 to 40% in size for all blends studied, independent of composition and solid mass fraction, after applying a shear rate of 300 s^{-1}. Therefore, the results of this work are in agreement with previous findings, although this time, at the nanoscale.

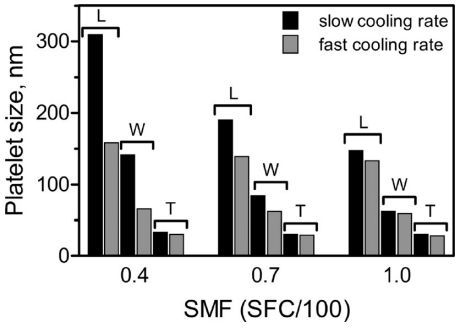

Figure 2. Example of the effect of crystallization under different cooling rates on the nanostructure of fats. Nanoplatelet lengths (L), widths (W), and thicknesses (T) for three non-interesterified (NI) fat blends, crystallized from the melt at two different cooling rates: slow (1 °C/min) and fast (10 °C/min) cooling rate. The standard error is ≤1.5% for all samples.

Changes in crystal thickness upon application of shear, obtained by the Scherrer analysis of the (001) small-angle X-ray reflection, displayed trends similar to that of nanoplatelet lengths and widths (Figure 1c). In both groups, NI and CI blends, the decrease in platelet thickness upon application of shear was approximately 60%, 54%, and 35% for solid mass fraction values of 1, 0.7, and 0.4, respectively. In all fat blends, despite the composition and crystallization process, the thickness of nanocrystals decreased with an increase in solid mass fraction.

Figure 2 shows the mean values of platelet size as a function of solid mass fraction for blends subjected to nonisothermal crystallization, under slow and fast cooling rates. A number of studies have reported a relationship between fast cooling rates

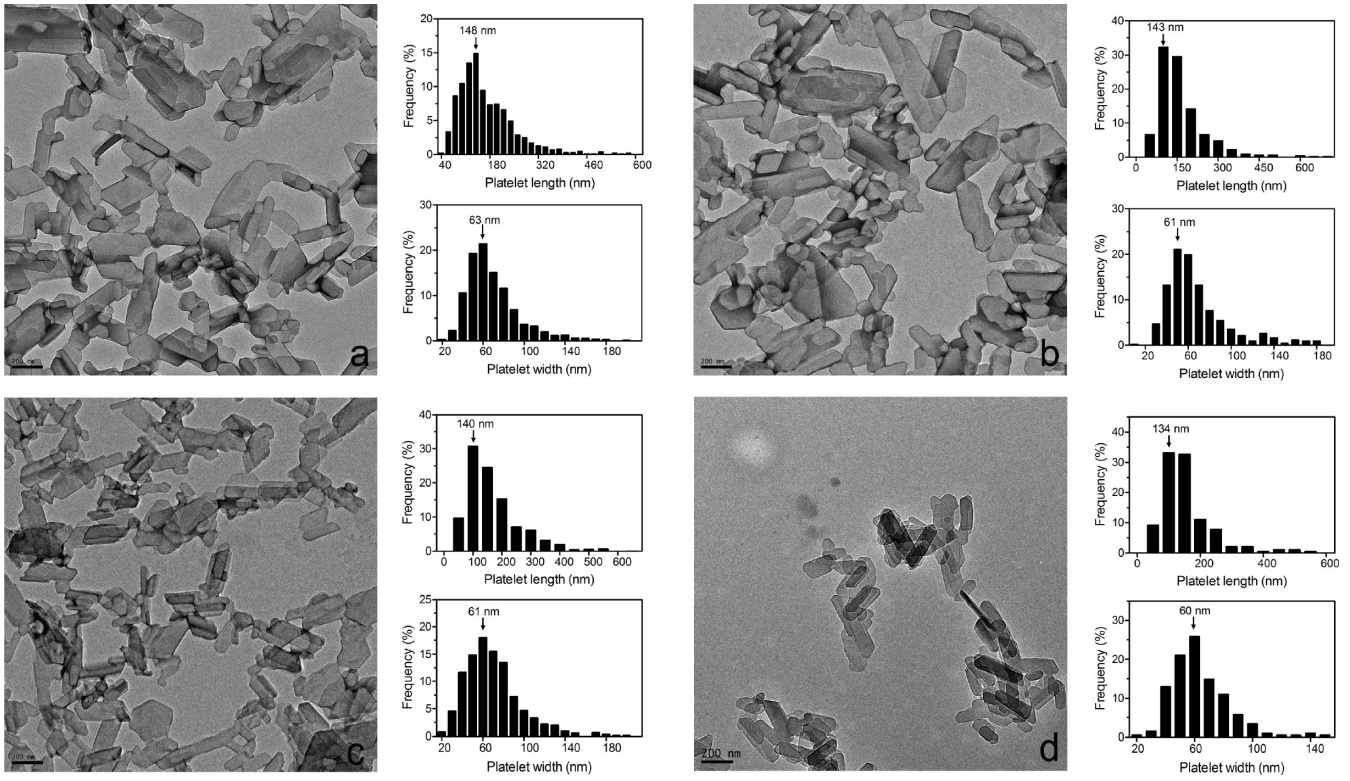

Figure 3. Cryo-TEM micrographs of tristearin (FHCO, solid mass fraction value ~1) subjected to interesterification and different external fields. (a) Static crystallization, (b) chemical interesterification and static crystallization, (c) crystallization under a laminar shear rate of 300 s^{-1}, and (d) static crystallization with a high cooling rate (10 °C/min). The corresponding length and width frequency distributions are shown to the right of each cryo-TEM image. The standard error is ≤1.5% in all samples.

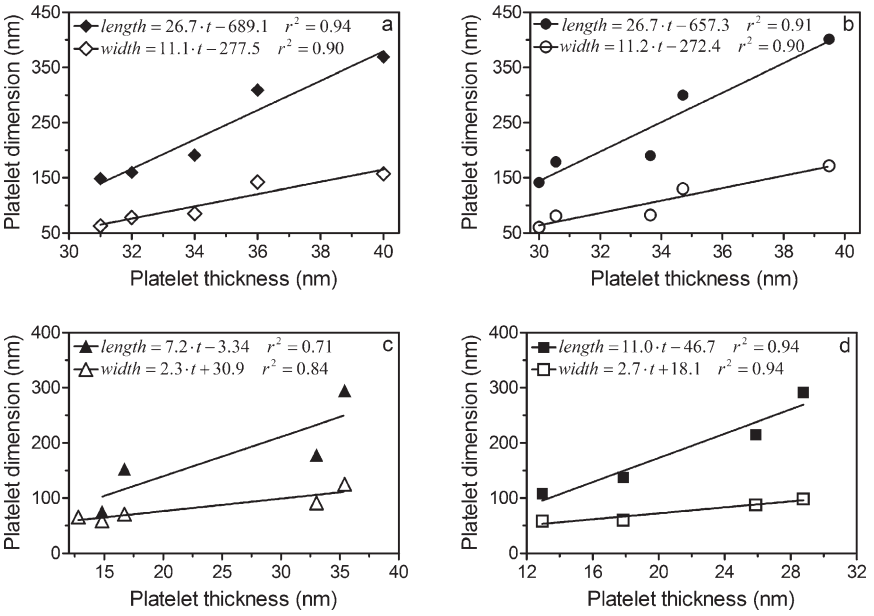

Figure 4. Relationship between platelet lengths and widths and their corresponding thicknesses (t) (symbols). The straight line and the equation in the graph represent the results of a linear regression on the data. The Pearson correlation coefficient (r^2) indicates the linearity of the data. NI (a) and CI (b) blends statically crystallized. NI (c) and CI (d) blends crystallized under shear.

and small crystal sizes at the microstructural level in fat crystal networks.[13,25,28,44,45] Not surprisingly, in this study, fat blends cooled at a high rate (10 °C/min) showed nanocrystal dimensions smaller than those observed in samples cooled slowly (1 °C/min). Faster cooling rates induced a decrease in platelet lengths and widths from 10% (in samples with 100% of FHCO; ~1 of solid mass fraction) to 50% (in samples with 50% of FHCO, 0.4 solid mass fraction), and from 5 to 10% in thickness, relative to the slow cooling rate ($P < 0.001$). The results showed that cooling rate affects fat blends in a more pronounced fashion at low supersaturation values. Enclosed below (A) for these findings could be that initially in the melt, the stacking of TAG chains and the formation of lamellar ordering is highly sensitive to the viscosity of the melt. As a consequence, at low solid mass fraction (and hence low viscosities) there is a high molecular mobility in the TAG melt which promotes nanocrystal growth. When a more drastic change in the supercooling conditions takes place, a high kinetic barrier is established and, as a consequence the growth of nanocrystals is restricted which leads to the formation of predominantly small nanoplatelets. At high solid mass fractions, there already is a high kinetic barrier, due to the high viscosity of the melt, which restricts the growth of the crystals. The contribution to the kinetic barrier from the fast cooling rate applied to the melt is small compared to the contribution from the high melt viscosity at high solid mass fractions. Thus, no large changes in crystal growth patterns are observed.

Figure 3 shows cryo-TEM micrographs corresponding to the 100% FHCO sample with a solid mass fraction value of ~1, which has been exposed to different crystallization conditions: NI, statically crystallized (a), CI, statically crystallized (b), NI, crystallized under laminar shear (c), and NI, fast cooled from the melt (d). In all samples, the cryo-TEM technique allows the observation of individual nanoplatelets after the solvent treatment. These platelets have a well-defined morphology in all the samples which indicates that there are no gross morphological alterations induced by interesterification or changes in crystallization conditions. The frequency distributions of particle lengths and widths along with the arithmetical median values are presented to the right of the corresponding micrographs. The cryo-TEM images along with the size distributions clearly indicate that interesterification had no significant effect on the dimensions of the extracted nanocrystals at equivalent solid mass fraction (Figure 3b). These results can be explained considering the proportion of FHCO and HOSO present in the sample. In this case, the fat sample consisted of 100% FHCO; therefore, its composition remained nearly constant after randomization. As a result, only a minor reduction in nanoplatelet size was observed. In addition, the interesterification process did not affect the morphology of the nanocrystals. As was observed before in Figure 1, shearing during crystallization induced a large decrease in platelet sizes (Figure 3c). Most nanoplatelets measured 148 nm × 63 nm under static crystallization conditions and diminished to 140 nm × 61 nm upon application of shear.

In the case of the same blend (100% of FHCO) crystallized at a fast cooling rate (10 °C/min), it is possible to observe smaller nanoplatelets than in those crystallized at a slow cooling rate (1 °C/min) (Figure 3d). Cooling rates strongly affected the nanoscale; the drop in nanoplatelet dimensions was 10% and 5% for length and width, respectively.

Figure 4 displays the relationship between platelet dimensions for NI and CI samples which were crystallized statically (Figure 4a,b) and under shear (Figure 4c,d). We discovered a linear relationship, with high correlation coefficients (r^2), between the length or width of the nanoplatelets and their thickness in all the blends. Another interesting observation arising from these results is that the linear regressions revealed nanoplatelet lengths of approximately twice the widths, in statically crystallized samples (Figure 4a,b). In sheared fat blends, this relationship between lengths and widths was 3 and 4, for NI and CI samples, respectively. These findings are very encouraging and interesting since they potentially would allow the prediction of platelet lengths and widths from the nanocrystal thickness which can be rapidly obtained by powder XRD.

It was encouraging to determine that the linear relationship between platelet dimensions was also observed for samples

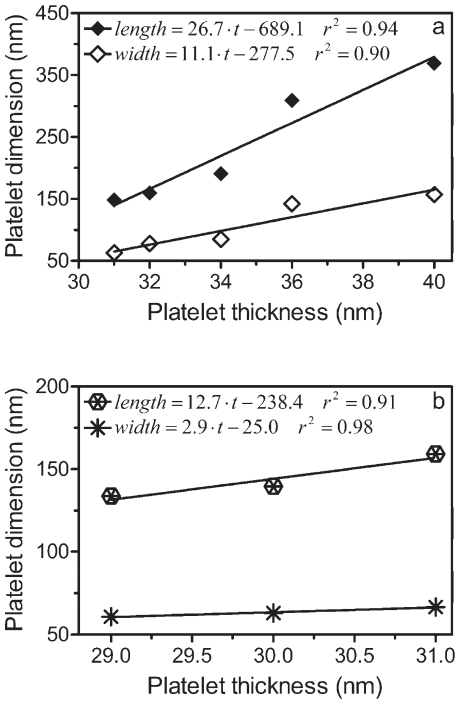

Figure 5. Relationship between platelet lengths and widths and their corresponding thicknesses (t). The straight line and the equation in the graph represent the results of a linear regression on the data. The Pearson correlation coefficient (r^2) indicates the linearity of the data. NI blends slow (a) and fast (b) cooled from the melt.

crystallized at different cooling rates (Figure 5). It is noteworthy to mention that in blends rapidly cooled from the melt, nanoplatelet lengths are ~4 times larger than widths (Figure 5b) compared with samples cooled slowly where platelet lengths are only ~2 larger than their corresponding widths (Figure 5a).

The linear correlation between nanocrystal dimensions confirms our previous observation that the nanoscale in fat crystal networks is composed of well-defined platelets with no considerable changes in morphology regardless of the composition and the strength of the applied external fields − only the dimensions are changed.

Conclusions

Here, we report that externally induced changes in composition and crystallization conditions in triacylglycerol crystal networks translate only into alterations in nanocrystal size while maintaining crystal morphology. This demonstrates that it is possible to engineer the functional properties of fats and fat-structured materials at the nanoscale by using external fields or chemical transformations, and even to predict the changes induced.

Acknowledgment. The authors thank The Natural Sciences and Engineering Research Council of Canada and Advanced Foods and Materials network for the financial support grant.

References

(1) Kromhout, D.; Menotti, A.; Bloemberg, B.; Aravanis, C.; Blackburn, H.; Buzina, R.; Dontas, A. S.; Fidanza, F.; Giampaoli, S.; Jansen, A..; et al. *Prev. Med.* **1995**, *24*, 308–315.
(2) Ascherio, A.; Rimm, E. B.; Giovannucci, E. L.; Spiegelman, D.; Stampfer, M.; Willett, W. C. *Br. Med. J.* **1996**, *313*, 84–90.
(3) Hu, F. B.; Stampfer, M. J.; Manson, J. E.; Rimm, E.; Colditz, G. A.; Rosner, B. A.; Hennekens, C. H.; Willett, W. C. *N. Engl. J. Med.* **1997**, *337*, 1491–1499.
(4) Salmerón, J.; Hu, F. B.; Manson, J. E.; Stampfer, M. J.; Colditz, G. A.; Rimm, E. B.; Willett, W. C. *Am. J. Clin. Nutr.* **2001**, *73*, 1019–1026.
(5) van den Tempel, M. J. *Colloid Interface* **1979**, *71*, 18–20.
(6) deMan, J. M.; Beers, A. M. *J. Texture Stud.* **1987**, *18*, 303–318.
(7) Chawla, P.; deMan, J. M. *J. Am. Oil Chem. Soc.* **1990**, *67*, 329–332.
(8) Vreeker, R.; Hoekstra, L. L.; den Boer, D. C.; Agterof, W. G. M. *Colloids Surf.* **1992**, *65*, 185−189.
(9) Heertje, I. *Food Microstruct.* **1993**, *12*, 77–94.
(10) Marangoni, A. G.; Rousseau, D. *J. Am. Oil Chem. Soc.* **1996**, *73*, 991–994.
(11) Narine, S. S.; Marangoni, A. G. *Phys. Rev.* **1999**, *59*, 1908–1920.
(12) West, A. R. In *Solid State Chemistry and Its Applications*; John Wiley & Sons: Chichester: West Sussex, England, 1984; pp 174.
(13) Campos, R.; Narine, S.; Marangoni, A. G. *Food Res. Int.* **2002**, *35*, 971–981.
(14) Noor Lida, H. M. D; Sundram, K.; Siew, W. L.; Aminah, A.; Mamot, S. *J. Am. Oil Chem. Soc.* **2002**, *79*, 1138–1143.
(15) Foubert, I.; Dewettinck, K.; Janssen, G.; Vanrolleghem, P. A. *J. Food Eng.* **2006**, *75*, 551.
(16) Rodriguez, A.; Castro, E.; Salinas, M. C.; Lopez, R.; Miranda, M. *J. Am. Oil Chem. Soc.* **2001**, *78*, 431–436.
(17) Narine, S. S.; Humphrey, K. L.; Bouzidi, L. *J. Am. Oil Chem. Soc.* **2006**, *83*, 913.
(18) Lida, A. M. D. N.; Sundram, K.; Siew, W. L.; Amina, A.; Mamot, S. *J. Am. Oil Chem. Soc.* **2002**, *79*, 1138.
(19) Piska, I.; Zárubová, M.; Louzecký, T.; Karami, H.; Filip, V. *J. Food Eng.* **2006**, *77*, 347.
(20) Ahmadi, L.; Wright, A. J.; Marangoni, A. G. *Eur. J. Lipid Sci. Technol.* **2008**, 1014–1024.
(21) Ahmadi, L.; Wright, A. J.; Marangoni, A. G. *Eur. J. Lipid Sci. Technol.* **2008**, *110*, 1025–1034.
(22) Mazzanti, G.; Guthrie, S. E.; Sirota, E. B.; Marangoni, A. G.; Idziak, S. H. J. *Cryst. Growth Des.* **2003**, *3*, 721–725.
(23) Hoerr, C. W. *J. Am. Oil Chem. Soc.* **1967**, *44*, 238A.
(24) Rousseau, D.; Marangoni, A. G.; Jeffrey, K. R. *J. Am. Oil Chem. Soc.* **1998**, *75*, 1833–1839.
(25) Herrera, M. L.; Hartel, R. W. *J. Am. Oil Chem. Soc.* **2000**, *77*, 1177–1187.
(26) Van Aken, G. A.; Visser, K. A. *J. Dairy Sci.* **2000**, *83*, 1919–1932.
(27) Martini, S.; Herrera, M. L.; Hartel, R. W. *J. Am. Oil Chem. Soc.* **2002**, *79*, 1055–1062.
(28) Litwinenko, J. W.; Rojas, A. M.; Gerschenson, L. N.; Marangoni, A. G. *J. Am. Oil Chem. Soc.* **2002**, *79*, 647–654.
(29) Pérez-Martínez, D.; Alvarez-Salas, C.; Charó-Alonso, M.; Dibildox-Alvarado, E.; Toro-Vazquez, J. F. *Food Res. Int.* **2007**, *40*, 47–62.
(30) Toro-Vazquez, J. F.; Dibildox-Alvarado, E.; Charó-Alonso, M.; Charó-Alonso, V.; Gómez-Aldapa, C. A. *J. Am. Oil Chem. Soc.* **2002**, *79*, 855.
(31) Acevedo, N. C.; Marangoni, A. G. *Cryst. Growth Des.* **2010**, DOI: 10.1021/cg100468e
(32) Campos, R. *In Fat Crystal Networks*; Marangoni, A. G., Ed.; Marcel Dekker: New York, 2005; Chapter 9, pp 267−348.
(33) deMan, J. M. *J. Dairy Res.* **1961**, *28*, 117–123.
(34) Rousseau, D.; Hill, A. R.; Marangoni, A. G. *J. Am. Oil Chem. Soc.* **1996**, *73*, 973–981.
(35) Ribeiro, A. P. B.; Grimaldi, R.; Gioielli, L. A.; Oliveira dos Santos, A.; Cardoso, L. P.; Goncalves, L. A. G. *Food Biophys.* **2009**, *4*, 106–118.
(36) Himavan, C.; Starov, V. M.; Stapley, A. G. F. *Adv. Colloid Interface Sci.* **2006**, *122*, 3.
(37) MacMillan, S. D.; Roberts, K. J.; Rossi, A.; Wells, M. A.; Polgreen, M. C.; Smith, I. *Cryst. Growth Des.* **2002**, *2*, 221–226.
(38) Mazzanti, G.; Guthrie, S. E.; Sirota, E. B; Marangoni, A. G.; Idziak, S. H. J. *Cryst. Growth Des.* **2004**, *4*, 409–411.
(39) Mazzanti, G.; Marangoni, A. G.; Idziak, S. H. J. *Phys. Rev. E* **2005**, 74.
(40) Kloek, W.; van Vliet, T.; Walstra, P. *J. Texture Stud.* **2005**, *36*, 544–568.
(41) Sonwai, S.; Mackley, M. R. *J. Am. Oil Chem. Soc.* **2006**, *83*, 583–596.
(42) Stapley, A. G. F.; Tewkesbury, H.; Fryer, P. *J. Am. Oil Chem. Soc.* **1999**, *76*, 677–685.
(43) MacMillan, S. D.; Roberts, K. J.; Rossi, A.; Wells, M. A.; Polgreen, M. C.; Smith, I. H. *Cryst. Growth Des.* **2003**, 221–226.
(44) Martini, S.; Herrera, M. L.; Hartel, R. W. *J. Am. Oil Chem. Soc.* **2002**, *79*, 1063–1068.
(45) Lopez, C.; Lesieur, P.; Bourgaux, C.; Ollivon, M. *J. Dairy Sci.* **2005**, *88*, 511–526.